

Multiple-scattering regime and higher-order correlations in x-ray-absorption spectra of liquid solutions

M. Benfatto and C. R. Natoli

*Istituto Nazionale di Fisica Nucleare, Laboratori Nazionali di Frascati, Casella Postale 13,
I-00044 Frascati (Roma), Italy*

A. Bianconi, J. Garcia,* A. Marcelli, and M. Fanfoni

Dipartimento di Fisica, Università degli Studi di Roma "La Sapienza," I-00185 Roma, Italy

I. Davoli

Dipartimento di Matematica e Fisica, Università degli Studi di Camerino, I-62032 Camerino, Italy
(Received 8 July 1985; revised manuscript received 12 May 1986)

By making a comparison between the Mn *K*-edge absorption of $(\text{MnO}_4)^-$ and $[\text{Mn}(\text{H}_2\text{O})_6]^{2+}$ complexes in aqueous solution we obtain an experimental determination of the energy extent of the type-II multiple-scattering (MS) regime that is substantially wider than expected. Theoretical calculations based on the MS formalism support this conclusion. We also recognize three energy regions in the absorption spectra of these complexes: a full MS region, where numerous or an infinite number of MS paths of high order contribute (depending on whether the MS series converges or not), an intermediate MS region, where only a few MS paths of low order are relevant, and a single-scattering region where the photoelectron is backscattered only once by the ligands [extended x-ray-absorption fine-structure (EXAFS) regime]. Theoretical considerations show that this must be a general situation in x-ray-absorption spectra and opens the way to a unified scheme for their interpretation. The energy extent of the three regions is obviously system dependent. We also show how to generalize to MS contributions the usual EXAFS analysis using curved-wave propagators and indicate how to extract geometrical information from the spectra of the two clusters investigated. In particular the method is used to derive the Mn—O—O—Mn path length in the $(\text{MnO}_4)^-$ complex.

I. INTRODUCTION

Interest in local structure determination beyond the pair distribution function has recently stimulated the growth of x-ray-absorption near-edge structure (XANES) studies, both from a theoretical and an experimental point of view.^{1,2} The reason for this lies in the fact that the low-energy side of an absorption spectrum is sensitive to the geometrical arrangement of the environment surrounding the absorbing atom, due to the generally strong scattering power of the atoms of the medium in this energy region which favors multiple-scattering (MS) processes (in principle, up to infinite order).^{3,4}

At energies such that the atomic scattering power becomes substantially small (in a way to be qualified later) a single-scattering (SS) regime takes place, where the modulation in the absorption coefficient [extended x-ray-absorption fine structure (EXAFS)] is substantially due to the interference effect of the outgoing photoelectron wave emanating from the photoabsorber and the wave backscattered by each surrounding atom.^{5,6} Hence this latter part of the spectrum provides information about the pair correlation function. By decreasing the photoelectron kinetic energy a gradual turnover takes place from the EXAFS SS regime to the XANES full MS (FMS) regime through a transition region where only low-order MS paths are expected to be relevant.^{7,8} This last intermediate MS (IMS) region has received attention in the literature mainly in connection with collinear atomic configuration

where the focusing effect makes collinear MS processes strong enough that they give an appreciable contribution even in the EXAFS region.^{6,9} For open structures, i.e., structures with no collinear configurations, it has been suggested that "the transition region terminates with the EXAFS region itself."¹⁰

More recently an interpretation of Cu *K* edge in terms of SS EXAFS theory with curved wave¹¹ and a Fourier analysis of the XANES region of KMnO_4 (Ref. 12) have suggested that in these systems the MS energy range is very small and have questioned the capability of XANES to probe high-order correlations.

It is the aim of this paper to critically assess the validity of these conclusions by presenting a unifying scheme of interpretation of x-ray-absorption spectra based on a precise mathematical approach and corroborated by experimental evidence.

At the same time a method of analysis is proposed capable in principle of providing higher-order correlation functions in some particular cases. The underlying idea is quite simple. Since the interpretation of XANES spectra is often complicated by the presence of higher-order neighbors, we have analyzed the absorption of single complexes in aqueous solution, consisting of a metal ion plus a first coordination shell of ligands, in order to remove the effect of unwanted higher-order shells.

In particular we have examined the Mn *K*-edge absorption spectra of $(\text{MnO}_4)^-$ and $[\text{Mn}(\text{H}_2\text{O})_6]^{2+}$ complexes. After rescaling of the energy scale to correct for the dif-

ferent metal ion ligand distance and a renormalization of the amplitude to account for the different numbers of first neighbors, the comparison between the two spectra shows the same sinusoidal behavior in that region of the photoelectron energy that is sensitive only to the pair correlation function (EXAFS region).

Any difference in the two spectra must then reflect a sensitivity of the photoelectron to the different geometrical arrangement of the ligand atoms around the metal ion in the two complexes. In this way we determine experimentally the extent of the energy region where information can be obtained about coordination geometry.

Based on this firm ground, we then turn to the theoretical analysis, in order to be able to derive quantitative information from the data. Using an exact expression for the absorption coefficient based on the MS theory, we show how to derive in a straightforward way the general term of the MS series with curved-wave propagators and at the same time give a precise mathematical criterion for its convergence.

When this criterion is satisfied we show that the absorption coefficient can be expressed as an absolutely convergent series whose n th term represents the contribution coming from the n th-order scattering paths. In particular the zeroth order represents the atomic absorption coefficient of the central absorbing atom, while the second is the EXAFS term with curved-wave propagators.

In the case of the complexes under consideration we show that the MS series is convergent for all energies above the Mn $1s$ - $3d$ transition. This fact allows us to subtract the atomic and EXAFS contribution from the experimental data and analyze the rest in terms of MS paths of higher order. The procedure parallels the one used by those who study neutrons for analyzing the anharmonic contribution to the vibrational scattering cross section after subtraction of the harmonic part from the spectrum. Due to the convergence of the MS series and various damping effects of the photoelectron in the final state one expects that only low-order scattering paths contribute to the absorption coefficient. In some fortunate cases, like $(\text{MnO}_4)^-$, it is possible in this way to extract a third-order correlation function over a range of more than 100 eV. As an application we derive the Mn—O(1)—O(2)—Mn path length in the $(\text{MnO}_4)^-$ cluster.

II. EXPERIMENTAL ANALYSIS

In order to obtain experimental evidence of the energy extent of the MS regime, as anticipated in the Introduction, we have measured the K -edge absorption spectra of 50 mM of MnCl_2 and KMnO_4 aqueous solutions with high resolution. The experiment was performed at the Frascati Synchrotron Radiation Facility. In both cases a 1 mm thick cell was used for transmission experiments. High resolution was achieved by using a Si(220) monochromator and an entrance slit of 0.5 mm. The storage ring Adone was operated at 1.5 GeV and 100 mA with a brilliance of about 10^9 photons/(sec mrad² mm² $10^{-4}\Delta E/E$). In the data analysis the pre-edge absorption background was subtracted.

Mn ion in solution is octahedrally coordinated by six H_2O molecules forming a stable $[\text{Mn}(\text{OH}_2)_6]^{2+}$ cluster

with Mn-O distance $d_1 = 2.17 \text{ \AA}$.¹³ The tetrahedral cluster $(\text{MnO}_4)^-$ is known instead to be quite stable in solution and its EXAFS has been analyzed by Rabe *et al.*¹⁴ to give a Mn-O distance $d_2 = 1.63 \text{ \AA}$. Only the contribution of the first shell is present for the photoelectron wave vector k above 5 \AA^{-1} in agreement with previous studies. In Fig. 1 the absorption spectra of $[\text{Mn}(\text{OH}_2)_6]^{2+}$ and $(\text{MnO}_4)^-$ are compared. The corresponding energy scales are in the ratio $(d_2^*/d_1^*)^2 = 0.47$ where d_2^* and d_1^* are the Mn-O distances in the two complexes, corrected for the linear term coefficient of the backscattering phase shift, in order to eliminate the effects in the spectra arising from the different bond length and the dependence of the phase shifts on the energy. The zero of the energy has been set at the first absorption feature ($1s$ - $3d$ transition) in both spectra. In this way the two spectra, after a further rescaling of the oscillating amplitude to take account of the different number of nearest neighbors (see inset in Fig. 1), show a superposed behavior in that energy region that contains information only about the pair correlation function (EXAFS). Below 160 eV (75 eV with reference to $[\text{Mn}(\text{OH}_2)_6]^{2+}$ scale) the absorption spectrum of $(\text{MnO}_4)^-$ deviates from the spectrum of $[\text{Mn}(\text{OH}_2)_6]^{2+}$ cluster. This fact is a clear indication that below these energies information about higher-order correlation functions or geometrical arrangement of the environment of the absorbing atom is contained in the spectra. Moreover the energy region where MS effects of type II (Ref. 12) are experimentally detectable is much wider than anticipated by various authors.

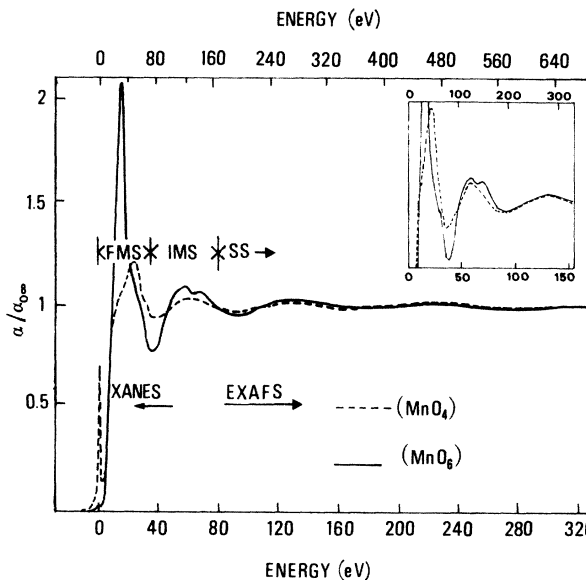


FIG. 1. Comparison between normalized Mn K -edge x-ray absorption spectra of $(\text{MnO}_4)^-$ and $[\text{Mn}(\text{OH}_2)_6]^{2+}$ ions from 50 mM aqueous solution of KMnO_4 and MnCl_2 . The respective energy scales are given in the upper (lower) part of the figure. The normalization is to a value $\alpha_{0\infty}$ of the atomic absorption at very high energy. A partition of the spectra in FMS (full MS), IMS (intermediate MS), and SS (single scattering) regions is sketched. The insert shows a comparison of the two spectra after a rescaling of the oscillating amplitudes in the ratio 4:6.

III. THEORETICAL CONSIDERATION

In order to get deeper insight into the MS region we have analyzed the spectra in the framework of MS concepts. In this formalism the polarization averaged absorption coefficient is given by^{6,11,15}

$$\alpha_F = \alpha_F^{l+1} + \alpha_F^{l-1} = A\hbar\omega N_0 [(l+1)M_{l,l+1}^2 X^{l+1} + lM_{l,l-1}^2 X^{l-1}], \quad (3.1)$$

where l is the orbital angular momentum of the initial core level ($l=0$ for K -shell excitation), $A = 16\pi^3/3(e^2/\hbar c)n_c$, where n_c is the density of absorbing atom, ω is the x-ray frequency, and $N_0 = mk/\pi^2\hbar^2$ is the free electron density of states, with k determined by the final-state kinetic energy E . The M 's are atomic-dipole transition matrix elements (radial part only) given by

$$M_{l,l\pm 1} = \int_0^\infty dr r^3 R_{l\pm 1}^0(r) \phi_{cl}(r), \quad (3.2)$$

where $\phi_{cl}(r)$ are initial core-level wave functions and $R_l^0(r)$ are regular solutions of the radial Schrödinger equation at energy E in the central muffin tin. They are normalized so that beyond the muffin-tin radius

$$R_l^0(r) \rightarrow j_l(kr) \cos\delta_l^0 + n_l(kr) \sin\delta_l^0, \quad (3.3)$$

where j_l and n_l are spherical Bessel and Neumann func-

tions, respectively, and δ_l^0 is the l -wave phase shift of the absorbing atom, assumed to be located at site 0. The interesting structural information in α_F is contained in the quantities X^l given by

$$X^l = 1/(2l+1) \text{Im} X^l = 1/[(2l+1) \sin^2\delta_l^0] \sum_m \text{Im}[(\mathbf{I} + \mathbf{T}_a \mathbf{G})^{-1} \mathbf{T}_a]_{lm,lm}^{00} \quad (3.4)$$

where \mathbf{I} is the unit matrix, $\mathbf{G} \equiv \mathbf{G}_{LL}^{jj}(1 - \delta_{ij})$ is the matrix describing the free spherical wave propagation of the photoelectron from site i and angular momentum $L = (l, m)$ to site j and angular momentum $L' = (l', m')$ and $\mathbf{T}_a \equiv (\mathbf{T}_a)_{LL'}^{jj} = \delta_{ij} \delta_{LL'} t_l^j$ is the diagonal matrix describing the scattering process of the photoelectron spherical wave with angular momentum l by the atom located at site i through the atomic dimensionless t -matrix element $t_l^j = \exp(i\delta_l^j) \sin\delta_l^j$, δ_l^j being the associated phase shift. Equation (3.4) implies that one must calculate the matrix

$$(\mathbf{I} + \mathbf{T}_a \mathbf{G})^{-1} \mathbf{T}_a = (\mathbf{T}_a^{-1} + \mathbf{G})^{-1} = \mathbf{T}$$

and then take the imaginary part of the matrix element $T_{lm,lm}^{00}$. The matrix \mathbf{T} plays the role of a \mathbf{T} matrix for the whole cluster and is constructed via the atomic \mathbf{T}_a matrix and the matrix of the propagators \mathbf{G} with matrix elements¹⁵

$$G_{LL'}^{jj} = \begin{cases} -4\pi i \sum_{L''} i^{l''+l-l'} C_L^{L' L''} h_{l''}^+(kR_{ij}) Y_{L''}(\hat{\mathbf{R}}_{ij}) & \text{if } (i \neq j), \\ 0 & \text{if } (i = j), \end{cases} \quad (3.5)$$

where $C_L^{L' L''}$ are the Gaunt coefficients, $h_l^+ = j_l + in_l$ is the usual Hankel function, and $Y_L(\hat{\mathbf{R}}_{ij})$ is a spherical harmonic of argument $\hat{\mathbf{R}}_{ij}$.¹⁶ Here $\mathbf{R}_{ij} = \mathbf{R}_i - \mathbf{R}_j$ is the vector joining the two atoms in the cluster located at site i and j , $\hat{\mathbf{R}}_{ij}$ being the associated versor and R_{ij} its modulus. Finally k is the photoelectron wave number. As apparent from Eqs. (3.4) and (3.5) the whole geometrical information on the medium around the photoabsorber is contained in the matrix inverse $(\mathbf{I} + \mathbf{T}_a \mathbf{G})^{-1}$. In absence of neighbors indeed, we have $\mathbf{G} \equiv \mathbf{0}$ and

$$X^l = 1/[(2l+1) \sin^2\delta_l^0] \sum_m \text{Im}[\mathbf{T}_a]_{lm,lm}^{00} = 1,$$

remembering that

$$[\mathbf{T}_a]_{lm,lm}^{00} = \exp(i\delta_l^0) \sin\delta_l^0.$$

Hence, from Eq. (3.1) the absorption coefficient reduces to the atomic absorption:

$$\alpha_F \rightarrow \alpha_F^a = A\hbar\omega N_0 [(l+1)M_{l,l+1}^2 + lM_{l,l-1}^2].$$

In XANES calculations the full MS result of Eq. (3.4) is compared with experimental spectra. However an alternative approach is viable, provided the condition $\rho(\mathbf{T}_a \mathbf{G}) < 1$ is verified for all relevant energies of interest, $\rho(\mathbf{A})$ indi-

cating the spectral radius of the matrix \mathbf{A} , i.e., the maximum modulus of its eigenvalues. In such a case

$$(\mathbf{I} + \mathbf{T}_a \mathbf{G})^{-1} = \sum_{n=0}^{\infty} (-1)^n (\mathbf{T}_a \mathbf{G})^n, \quad (3.6)$$

where the series on the right is absolutely convergent relative to some matrix norm. Insertion of this expression in Eq. (3.1) gives

$$\alpha_F = \alpha_F^{l+1} + \alpha_F^{l-1} = \sum_{n=0}^{\infty} \alpha_n^{l+1} + \sum_{n=0}^{\infty} \alpha_n^{l-1},$$

where

$$\alpha_0^{l+1} = A\hbar\omega N_0 (l+1) M_{l,l+1}^2, \quad \alpha_0^{l-1} = A\hbar\omega N_0 l M_{l,l-1}^2$$

and

$$\alpha_n^l = \alpha_0^l (-1)^n / [(2l+1) \sin^2\delta_l^0] \sum_m \text{Im}[(\mathbf{T}_a \mathbf{G})^n \mathbf{T}_a]_{lm,lm}^{00}. \quad (3.7)$$

Clearly $\alpha_0^{\pm 1}$ is the partial atomic absorption coefficient of the photoabsorber from an l initial state, whereas $\alpha_n^{\pm 1}$ represents the partial contribution of order n to the absorption coefficient of the entire cluster, coming from all

the processes where the photoelectron has been scattered $n - 1$ times by the surrounding atoms before returning to the photoabsorber at site 0 to exit into free space.

In this way it is possible to generate the MS series for the whole cluster. It is important to notice that the condition $\rho(\mathbf{T}_a \mathbf{G}) < 1$ is essential for the numerical equivalence of both sides of Eq. (3.6), hence for the MS series to be meaningful. Usually at very high energy this condition is satisfied since the modulus of the atomic t matrix goes to zero as k goes to infinity. At lower energies and in the near-edge region this condition is to be verified for the particular system under study. For our complexes this is the case for all energies greater than a lower bound E_m , which is located just below the rising edge. Hence an

analysis of the experimental spectra in terms of the quantities α_n^l is possible. Notice that $\alpha_1^l = 0$, since $\mathbf{G}_{LL}^{00} = 0$ and that α_2^l is the usual EXAFS term X_2^l times α_0^l , calculated with spherical wave propagators. In fact from Eq. (3.8) we find

$$\alpha_2^l = \alpha_0^l / (2l + 1) \sum_{j,m} \sum_{l',m'} \text{Im}[\exp(2i\delta_l^0) \mathbf{G}_{lm,l'm'}^{0j} t_l^j \mathbf{G}_{l'm',lm}^{j0}] . \quad (3.8)$$

Remembering the expression for the Gaunt coefficient in terms of the 3- j symbols¹⁶ and their orthogonality relations it is straightforward to rewrite Eq. (3.8) as

$$X_2^l = \alpha_2^l / \alpha_0^l = \text{Im} \left\{ \exp(2i\delta_l^0) \sum_{j(\neq 0)} \sum_{l'} (2l' + 1) t_l^j \sum_{l''} (2l'' + 1) \left[\begin{matrix} l & l' & l'' \\ 0 & 0 & 0 \end{matrix} \right] h_{l''}^+(kR_{0j}) \right\}^2$$

recovering the well-known result.¹¹

It is possible to write down more cumbersome expressions for the higher-order terms α_n^l ($n > 2$) using the $(3n - 3)$ - j symbols. However their practical usefulness decreases with increasing order. It is much faster to generate them by using a MS program which already calculates the matrix $\mathbf{I} + \mathbf{T}_a \mathbf{G}$. With a little more computing labor, the program can be modified so that the matrix inversion is performed either exactly or through the series expansion Eq. (3.6). This latter method automatically generates the quantities α_n^l of Eq. (3.7).

For future use we only notice that a general expression for these quantities can be written down immediately. We find in fact

$$X_n^l = \alpha_n^l / \alpha_0^l = \sum_{p_n} \mathbf{A}_n^l(k, R_{ij}^{p_n}) \sin [kR_{p_n} + \Phi_n^l(k, R_{ij}^{p_n}) + 2\delta_l^0] , \quad (3.9)$$

where \sum_{p_n} indicates the sum over all paths p_n of order n starting from and ending at the central photoabsorbing atom with $n - 1$ intermediate steps on the neighboring atoms, R_{p_n} indicates the corresponding total path length and the dependence of the amplitude and the phase functions $\mathbf{A}_n^l(k, R_{ij}^{p_n})$ and $\Phi_n^l(k, R_{ij}^{p_n})$ is on some rotationally invariant combination of scalar and vector products of vectors joining consecutive site location with the path, symbolically denoted by $R_{ij}^{p_n}$.

Their expression is easily obtained from Eq. (3.7) through the relation

$$\mathbf{A}_n^l \exp(\Phi_n^l) = (-1)^n \exp(-2i\delta_l^0) / [(2l + 1) \sin^2 \delta_l^0] \times \sum_m \text{Im}[(\mathbf{T}_a \mathbf{G})^n \mathbf{T}_a]_{lm,lm}^{00} , \quad (3.10)$$

where the matrix elements $\mathbf{G}_{LL'}^{ij}$ are related to the $\mathbf{G}_{LL'}^{ij}$'s by

$$G_{LL'}^{ij} = \begin{cases} \exp(-ikR_{ij}) G_{LL'}^{ij} & \text{if } i, j \in p_n \\ 0 & \text{if } i \text{ or } j \notin p_n \end{cases}$$

Equations (3.9) and (3.10) represent the generalization of the usual EXAFS formula to the higher-order terms in the MS series. When the experimental X_n^l are available one can extend to this more general case the analysis used for the EXAFS signal. We shall show an application of this in the following.

All the preceding considerations apply for a real single-particle potential. The extension to a complex absorptive potential is not so simple and will be treated in a subsequent paper.

We have chosen instead to convolute the calculated spectra with a Lorentzian broadening function. This procedure, usually followed in the literature,^{2,17} accounts satisfactorily for inelastic processes and finite lifetime effects.

IV. COMPARISON BETWEEN THEORY AND EXPERIMENT

In this section we compare the calculated and the experimental spectra for the $(\text{MnO}_4)^-$ and $[\text{Mn}(\text{H}_2\text{O})_6]^{2+}$ complexes. In both cases, to evaluate the atomic phase shifts, we have used two kinds of single-particle potentials: the ordinary $X\alpha$ energy-independent potential obtained through the usual Mattheiss prescription¹⁸ for the muffin-tin approximation and the real part of the complex energy-dependent Hedin-Lundqvist (HL) potential¹⁹ constructed by using the electron density obtained in the same approximation. Hydrogen atoms were neglected in the $[\text{Mn}(\text{H}_2\text{O})_6]^{2+}$ cluster.

The agreement with experimental data is surprisingly good with respect to the shape of the spectrum for both potentials. It is not as good in reference to the location of the high-energy maxima in the case of $X\alpha$ potential. In such a case, to get agreement it was necessary to contract the experimental energy scale by a factor 0.9. However the calculation based on the HL potential corrected for this discrepancy, which then was due to the energy independence of the $X\alpha$ potential. For the following com-

parisons we then discarded this latter potential in favor of the more physical HL potential. Notice however that for all practical purposes the quantities α_F and α_n calculated by using the HL potential coincide with the corresponding quantities based on the $X\alpha$ potential when plotted versus a contracted energy scale.

Figure 2 shows such a comparison for the $[\text{Mn}(\text{H}_2\text{O})_6]^{2+}$ complex. In Fig. 2(a) the quantity α_F^c is the calculated absorption coefficient obtained by exact inversion of the MS matrix. The superscript c indicates convolution by an energy-dependent Lorentzian broadening function with

$$\Gamma_{\text{tot}}(E) = \Gamma_h + \Gamma_{\text{expt}} + \Gamma_{\text{el}}(E),$$

where $\Gamma_h = 0.5$ eV is the core-hole width, $\Gamma_{\text{expt}} = 1$ eV is the experimental resolution, and $\Gamma_{\text{el}}(E)$ (of the order of 2.5 eV) is a slowly varying energy-dependent damping for the electron in the final state, taken from the imaginary

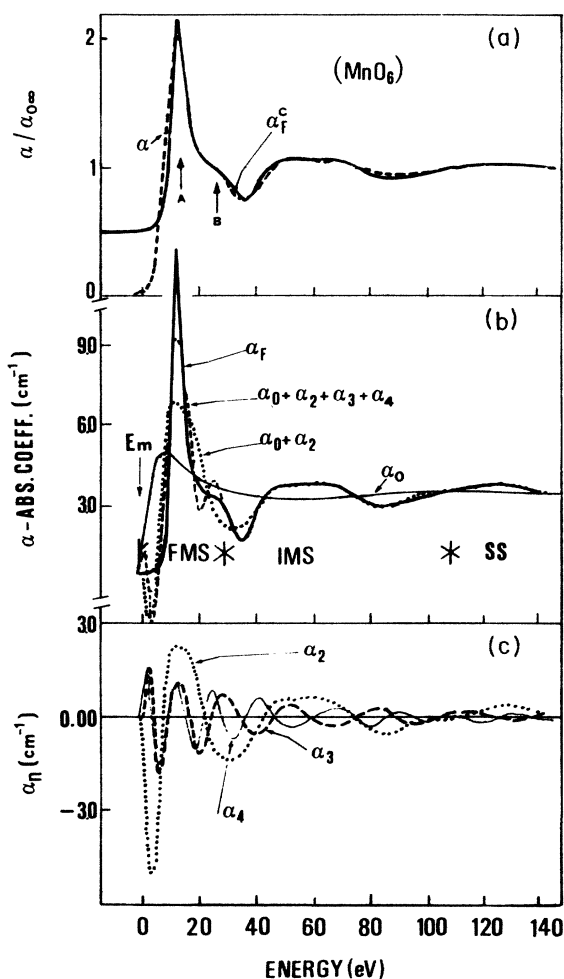


FIG. 2. (a) Comparison between experimental (α) and calculated (α_F^c) spectra for the $[\text{Mn}(\text{OH}_2)_6]^{2+}$ cluster. The calculated curve has been convoluted with an energy-dependent Lorentzian broadening function. (b) Breakdown of the calculated bare spectrum α_F into partial contributions $\sum_{n=0}^N \alpha_n$ for $N=0, 2, 4$. E_m indicates the lowest energy bound for the MS expansion to be valid. To obtain cross section in Mb divide by 30.1. (c) MS contributions of n th order to the absorption coefficient.

part of the complex HL potential. Figures 2(b) and 2(c) show the breakdown of α_F in terms of the partial contributions α_n for n up to 4. Apart from minor deviations, the sum $\alpha_0 + \alpha_2$ is already a good approximation to α_F for energies greater than 40 eV. So it would seem that the EXAFS regime starts at this point. The agreement is however deceiving and is due to a fortuitous cancellation of the α_3 and α_4 contributions which are quite sizable and comparable in magnitude with α_2 in the whole energy range considered, but opposite in phase with each other [Fig. 2(c)]. This fact is due both to the geometry (existence of collinear paths of order 3 and 4) and to the particular value of the $l=1$ phase shift of the absorbing atom ($\approx \pi$) in the range 40–80 eV. At lower energies (0–40 eV) contributions of MS paths coming from α_3 and α_4 are evident for features A and B. In particular peak A gets contributions from all MS processes which, due to the particular geometrical coordination, happen to be all in phase at one particular energy (resonance energy). In this sense peak A is a resonance feature.

Figure 3 shows the same comparison for the $(\text{MnO}_4)^-$ cluster. In this case $\alpha_0 + \alpha_2 + \alpha_3$ is enough to get good agreement with α_F in the range 50–140 eV and in this interval α_n ($n \geq 4$) is negligible. Below 50 eV MS contributions of an order higher than 3 are essential to get the spectral features A and B. As before B can be considered a broad resonance. The breakdown approach in terms of partial contributions to the absorption coefficient shows the continuous merging of the MS regime into the SS re-

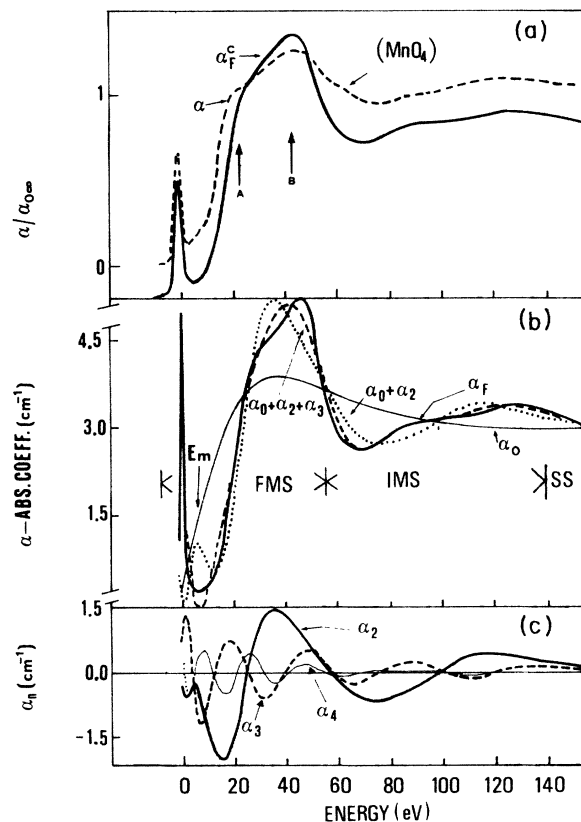


FIG. 3. Same as Fig. 2, for the $(\text{MnO}_4)^-$ cluster.

gime. However the merging interval is much larger than previously suspected. It ranges from 50 to 150 eV in $(\text{MnO}_4)^-$. Due to the convergence of the MS series the higher energy, the lower is the order of the correlation functions probed by the photoelectron. Damping considerations also corroborate this conclusion since damping increases the rate of convergence. As a general rule, theory indicates that the n th-order contribution α_n to the absorption coefficient scales as $N_n(R)^{-n}e^{-n\lambda R}$, where R is the length scale of the cluster of atoms under consideration, $\lambda^{-1} = \text{Im}(E_{el} + i\Gamma_{\text{tot}})^{-0.5}$ is the mean free path for the photoelectron in the final state, including core-hole lifetime and experimental broadening (typically of the order of 4–10 Å in the energy range 20–200 eV above the ionization edge, depending on the material under consideration), N_n is the multiplicity of the MS paths contributing to α_n . This rule can serve as a guideline to estimate the order of n that is accessible to experiments. More quantitatively the effect of damping on the α_n 's, estimated by performing a Lorentzian convolution with $\Gamma_{\text{tot}}(E)$, results in an amplitude reduction of about 25%.

In closing this section we remark that the agreement with experiment is significantly worse for MnO_4 than for the MnO_6 cluster. Part of the reason, we believe, is due to the poor approximation of the real potential by the muffin-tin model in the case of tetrahedral (open) structure. A further source of discrepancy can arise from the effect of a second coordination shell, averaged over many configurations in the solution, which is likely to be more relevant for an open structure than for a closed-packed arrangement. These points are presently under investigation.

V. THE INTERMEDIATE MS REGION

The above comparison between calculated and experimental spectra of the MnO_4 and MnO_6 cluster shows convincing evidence that MS effects of type II (noncollinear configuration) in the sense of Bunker and Stern¹² exist and are experimentally detectable well beyond the limits indicated in their paper. It is also rewarding that the theory supports the experimental evidence as to the energy extent of the MS region.

We want to show in this section how to exploit these effects to extract information on the geometrical arrangement around the photoabsorber. As apparent from the considerations of Sec. IV, it is in the tetrahedral cluster that deviations from pure EXAFS behavior first begin to show. This is a rather fortunate case, in that for a large energy range (≈ 100 eV) those deviations are caused only by the α_3 term, the higher-order terms being negligible. By exploiting our *a priori* knowledge of the α_0 and α_2 terms, we have subtracted the calculated X_2 contribution, conveniently convoluted, from the measured spectrum normalized to α_0 . The resulting signal is shown in Fig. 4(a) where it is compared with the calculated α_3 . The agreement is striking, confirming our initial guess. More details about the procedure to extract the signal are given in Ref. 20 where the same encouraging results are obtained for the chromate cluster $(\text{CrO}_4)^{2-}$. The signal so extracted is clearly a measure of a three-particle correlation function and bears information on the relative posi-

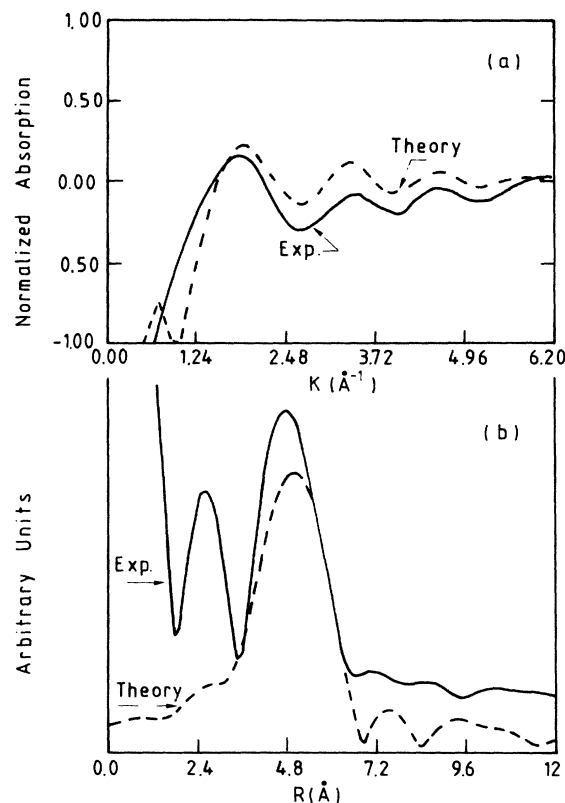


FIG. 4. (a) Comparison between normalized theoretical $X_3 = \alpha_3/\alpha_0$ signal (dashed line) and experimental signal (solid line), obtained as described in the text, for the $(\text{MnO}_4)^-$ cluster. The threshold energy E_0 has been set at the first absorption peak. (b) Comparison of theoretical and experimental Fourier transformed signals.

tion of the central metal ion with respect to any two oxygen ligands. The absence of beating phenomena in the signal is an indication that all the twelve third-order paths have the same total length, pointing to an undistorted tetrahedral coordination. The associated period is obviously related to the perimeter of the triangular paths through Eq. (3.9). The Fourier transform of the theoretical and the experimental signals are shown in Fig. 4(b), whereas the calculated amplitude and the phase function $A_3^l(k, R_{ij}^3)$ and $\Phi_3^l(k, R_{ij}^3)$ are plotted in Fig. 5. Here phase oscillations around an averaged constant slope of about $\alpha_1 = -0.85$ Å reflect amplitude modulations. As for the EXAFS analysis the true path length R_t lies at $R_t = R_f - \alpha_1$ where R_f is the observed maximum in the Fourier transform, which is at 5 Å for the “theoretical” signal and 4.8 Å for the “experimental” one. Hence we derive for the length of the path a “theoretical” value of 5.85 Å and an “experimental” value of 5.65 Å, in opposition to a real value of 5.87 Å. The discrepancy with the “experimental” value might be due to an inaccuracy of the subtraction procedure or may reflect physical reasons, e.g., effects of vibrational bending modes which we have not taken into account. This point is being investigated.

The same procedure cannot be followed for the MnO_6 cluster, because of the fortuitous cancellation of the α_3

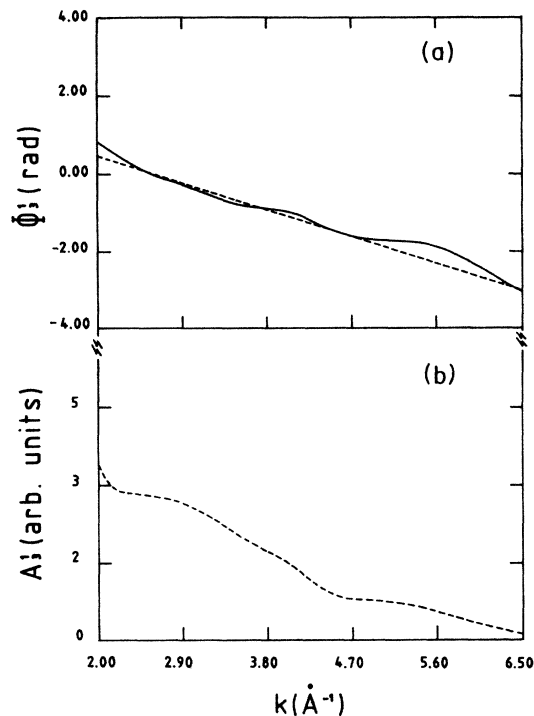


FIG. 5. (a) Phase function Φ_3^1 for third-order scattering path in the $(\text{MnO}_4)^-$ cluster (solid curve). The straight line (dashed line), obtained by a least-square-fitting procedure, gives an indication of the average slope of Φ_3^1 . (b) The associated amplitude function A_3^1 in arbitrary units.

and α_4 signals over a range of nearly 100 eV. However this simple fact imposes a stringent constraint on the geometrical coordination of the ligands around the metal ion. In fact, even using the curved-wave propagators, it is possible to show²¹ that to leading order, the α_n contributions to the unpolarized absorption coefficient are proportional to $\cos\beta$ where β is the angle between the first and the last scattering path. The same property rigorously holds instead in the plane-wave approximation.²² Now the fact that α_3 and α_4 almost cancel indicates that only collinear paths survive and consequently any two noncollinear vectors joining the central atom to the ligands must be at right angle, the whole complex being centrosymmetric. This fact, together with the added information, derived by EXAFS analysis, that there are six neighbors at equal distance from the center, points immediately to an octahedral coordination.

Even though a look at the shape of the spectrum near threshold is often sufficient to establish this fact, it is re-

warding that a deeper analysis leads to the same conclusion.

VI. DISCUSSION AND CONCLUSIONS

We have shown that MS effects play a nonnegligible role in a large energy range of the photoabsorption spectrum and that, at least in the particular cases we have studied, they are exploitable to extract geometrical information on the systems under investigation. It is tempting to generalize the picture that emerges from the above considerations. Figures 1, 2, and 3 clearly show that one can distinguish three regions in a photoabsorption spectrum: a FMS region, where numerous or an infinite number of MS paths of high order contribute to its final shape (depending on whether the MS series converges or not), followed by an IMS region where only a few MS paths of low order are relevant (typically $n \leq 4$), this region merging continuously into the EXAFS regime (SS region). This picture is supported by theoretical considerations. In fact the spectral radius $\rho(\mathbf{T}_a \mathbf{G})$ is a continuous function of the energy, going to zero as k goes to infinity and tending to infinity as k goes to zero, due to the singularity of the Hankel function $h_l^+(kR_{ij})$ in Eq. (3.5) at $k=0$. Moreover, the nearer one is to its value, the slower the convergence of the series, the point $\rho=1$ separating the region of convergence from that of nonconvergence. These properties immediately entail the existence of the three regions mentioned above. Obviously the energy extent of each region is system dependent and one needs to study many cases to see where the balance is stuck between them. Also the introduction of a complex potential modifies this balance toward depressing higher-order terms and pushing to lower energies the point at which $\rho=1$.

However the important fact to keep in mind is the convergence of the MS series if one wants to analyze the spectrum by the Fourier transform method. There is no *a priori* guarantee that in the region of nonconvergence one can parametrize the data by the functional form Eq. (3.9) or a series of these functions. In this latter case a different method of analysis must be devised.

Finally, in concluding, we remark that for EXAFS analysis based on phase transferability from reference models, octahedral clusters are to be preferred to tetrahedral ones in the range 40–150 eV.

ACKNOWLEDGMENTS

The experimental work was performed at the Frascati Synchrotron Radiation Facility run under a joint agreement by Consiglio Nazionale delle Ricerche (CNR) and Istituto Nazionale di Fisica Nucleare.

*Permanent address: Departamento de Termologia, Universidad de Zaragoza, E-50009 Zaragoza, Spain.

¹EXAFS and Near Edge Structure, Vol. 27 of *Springer Series in Chemical Physics*, edited by A. Bianconi, L. Incoccia, and S. Stipich (Springer, Berlin, 1983).

²F. W. Kutzler, C. R. Natoli, D. K. Misemer, S. Doniach, and

K. O. Hodgson, *J. Chem. Phys.* **73**, 3274 (1980).

³P. J. Durham, J. B. Pendry, and C. H. Hodges, *Solid State Commun.* **38**, 159 (1981).

⁴A. Bianconi, M. Dell'Ariccia, P. J. Durham, and J. B. Pendry, *Phys. Rev. B* **26**, 6502 (1982).

⁵D. E. Sayers, E. A. Stern, and F. W. Lytle, *Phys. Rev. Lett.* **27**,

- 1204 (1971).
- ⁶P. A. Lee and J. B. Pendry, *Phys. Rev. B* **11**, 2795 (1975).
- ⁷C. R. Natoli, in *EXAFS and Near Edge Structure*, Ref. 1, p. 43.
- ⁸A. Bianconi, *EXAFS and Near Edge Structure III*, Vol. 2 of *Springer Proceedings of Physics*, edited by K. O. Hodgson, B. Hedman, J. E. Penner-Hahn (Springer, Berlin, 1984), p. 167.
- ⁹B. K. Teo, *EXAFS and Near Edge Structure*, Ref. 1, p. 11.
- ¹⁰J. B. Pendry, in *EXAFS and Near Edge Structure*, Ref. 1, p. 4.
- ¹¹J. E. Müller and W. L. Schaich, *Phys. Rev. B* **27**, 6489 (1983); W. L. Schaich, *ibid.* **29**, 6513 (1984).
- ¹²G. Bunker and E. A. Stern, *Phys. Rev. Lett.* **52**, 1990 (1984).
- ¹³G. Licheri and G. Pinna, in *EXAFS and Near Edge Structure*, Ref. 1, p. 240.
- ¹⁴P. Rabe, G. Tolkiehn, and A. Werner, *J. Phys. C* **12**, 1173 (1979).
- ¹⁵P. J. Durham, J. B. Pendry, and C. H. Hodges, *Comput. Phys. Commun.* **25**, 193 (1982); P. Lloyd and P. W. Smith, *Adv. Phys.* **21**, 69 (1972).
- ¹⁶A. R. Edmonds, *Angular Momentum In Quantum Mechanics* (Princeton University, Princeton, NJ, 1974).
- ¹⁷J. E. Muller, O. Jepsen, and J. W. Wilkins, *Solid State Commun.* **42**, 365 (1982).
- ¹⁸L. Mattheiss, *Phys. Rev.* **134**, A970 (1964).
- ¹⁹L. Hedin and B. I. Lundqvist, *J. Phys. C* **4**, 2064 (1971).
- ²⁰J. Garcia, M. Benfatto, C. R. Natoli, A. Bianconi, A. Marcelli, and I. Davoli, *Solid State Commun.* **58**, 595 (1986).
- ²¹M. Benfatto and C. R. Natoli (unpublished).
- ²²J. J. Boland, S. E. Crane, and J. D. Baldeschwieler, *J. Chem. Phys.* **77**, 142 (1982).